This is the accepted manuscript made available via CHORUS. The article has been published as:

Millikelvin measurements of permittivity and loss tangent of lithium niobate

Silvia Zorzetti, Changqing Wang, Ivan Gonin, Sergey Kazakov, Timergali Khabiboulline, Alexander Romanenko, Vyacheslav P. Yakovlev, and Anna Grassellino

Phys. Rev. B **107**, L220302 — Published 15 June 2023

DOI: 10.1103/PhysRevB.107.L220302

Millikelvin measurements of permittivity and loss tangent of lithium niobate

Silvia Zorzetti,[1,*] Changqing Wang,[1] Ivan Gonin,[1] Sergey Kazakov,[1] Timergali Khabiboulline,[1] Alexander Romanenko,[1] Vyacheslav P Yakovlev,[1] and Anna Grassellino[1]

[1] *Fermi National Accelerator Laboratory, Batavia, IL 60510, USA*

Lithium Niobate is an electro-optic material with many applications in microwave signal processing, communication, quantum sensing, and quantum computing. In this letter, we present findings on evaluating the complex electromagnetic permittivity of lithium niobate at millikelvin temperatures. Measurements are carried out using a resonant-type method with a superconducting radio-frequency (SRF) cavity operating at 7 GHz and designed to characterize anisotropic dielectrics. The relative permittivity tensor and loss tangent are measured at 50 mK with unprecedented accuracy.

Introduction. Lithium Niobate (LN: $LiNbO_3$) is a nonlinear ferroelectric material with rich optical, acoustic, and piezoelectric properties [1]. Because of the large electro-optic coefficient ($r33 = 31$ pm/V at 9 GHz), it is of great interest in various applications spanning from communication, microwave-optical transduction, biomedical devices to sensing [2–7]. As a basic element of an electro-optic modulator (EOM), LN modulates an incoming optical career signal by the amplitude of an applied voltage due to the Pockels effect. Optical cavities made of LN can perform with a high quality (Q) factor in the range of $10^6 - 10^8$ [8]. This is possible through high-quality chemical and mechanical polishing of the surfaces. Such optical cavities can operate in whispering gallery modes, where a three-wave mixing process can occur between two optical modes and a microwave mode under the phase-matching condition [9]. Single-photon level measurements at millikelvin temperatures have demonstrated the ability of LN to maintain good electro-optic modulation properties in this regime [3, 10, 11]. Furthermore, the piezoelectric properties of LN allow the coupling between the electric signal and the mechanical degree of freedom, leading to intriguing phenomena in piezo-optomechanics [12]. Therefore, LN can be exploited to design physical devices to leverage the interaction between microwave, mechanical, and optical fields, which operate at intrinsically disparate frequencies.

Among the few materials exhibiting the Pockels effect and piezoelectric property, LN is one of the most employed in emerging applications in quantum computing and sensing for the coherent transduction of single photons [10, 12] and for enhancing the sensing capabilities of quantum sensors. These applications rely on bulk LN in three-dimensional (3D) hybrid systems or thin-film LN compatible with integrated two-dimensional (2D) devices. While several studies exist on the properties of LN crystals at room or higher temperatures [13–16], there is a need to gain more knowledge of the complex electromagnetic permittivity at cryogenic and millikelvin temperatures. Electromagnetic characterization of such dielectric crystals is necessary to understand their behavior under applied electromagnetic fields and, therefore, to design and devise many quantum computing and sensing applications and evaluate performance accurately. Goryachev et al. have determined the loss tangent of lithium niobate in the order 10^{-5} at the single photon level [17]. Besides, Wollack et al. studied the loss mechanisms of thin-film LN, including the resonant two-level-system (TLS) decay, the off-resonant TLS relaxation damping, and the temperature-independent mechanical loss at cryogenic temperatures [18]. In this letter, we present the measurement results of the complex dielectric properties of bulk LN crystals for 3D electro-optic applications at the quantum threshold with reduced uncertainty.

Methods. Superconducting radio-frequency (SRF) cavities are developed in high energy physics (HEP) to accelerate particle beams up to the speed of light. Such cavities can also achieve very high quality factors ($Q > 10^{10}$) at millikelvin temperatures [19, 20]. Because of the low microwave loss, SRF cavities are valuable tools for characterizing dielectric materials with high accuracy [21–23]. Here, an SRF cavity made of aluminum is designed and manufactured to study the loss tangent and the permittivity of bulk samples of lithium niobate or other ferroelectric materials (Fig. 1). The cylinder-shaped cavity hosts a cubic sample[1] of a z-cut LN. Alignment features are used to place the sample at the center of the cavity.

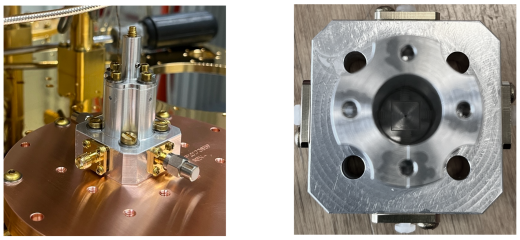


FIG. 1. *Left:* Sample holder cavity in a dilution refrigerator (DR). *Right:* Top view of the cavity with alignment features during installation of the LN crystal.

* email: zorzetti@fnal.gov

[1] The sample is made of pure single-crystal LN and has a dimension of $6 \times 6 \times 6$ mm. The z-cut surfaces are polished with surface quality of 20/10 scr/dig, flatness of $\lambda/8$, and parallelism < 20 arcsec.

The cavity is equipped with four lateral variable antenna couplers (Fig 2(a)). Loop antenna probes are used to couple to modes with different polarizations. The bulk sample is not glued, it is held in position through a spring-loaded sapphire rod that compensates for thermal shrinkage during cooldown, allowing to keep a constant force on the sample from room temperature through cryogenic temperature, and improves the thermal conductivity between the sample and the cavity. Sapphire is a dielectric material with a negligible loss tangent compared to the sample under test. Specifically, the loss tangent of sapphire is $\sim 10^{-8}$ at low temperatures [24, 25]. The diameter of the holder is selected in such a way that there is no radiation trough the holder pipe at the operating frequencies. The cavity is installed in a dilution refrigerator (DR) and cooled down to millikelvin. The schematic view of the experiment in the DR is shown in Fig. 2(b). As the environmental conditions, such as temperature or microwave power, vary, the changes in the quality factor and the frequency shifts are monitored to evaluate the dielectric permittivity and the crystal's loss tangent.

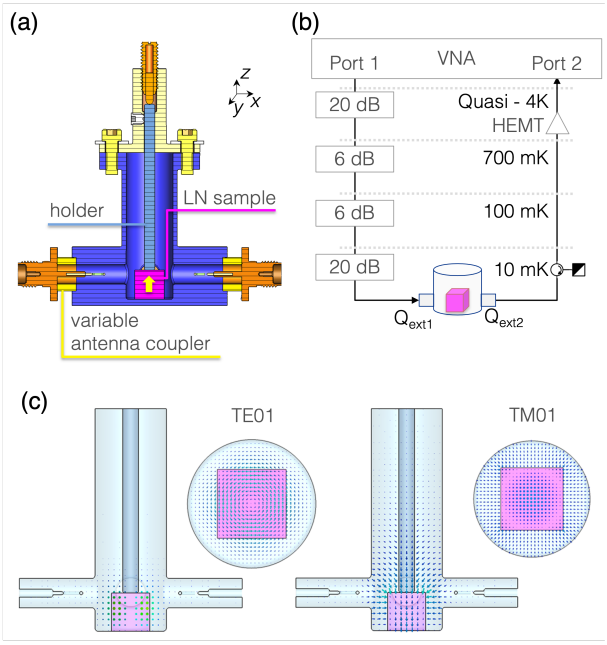


FIG. 2. **(a)** Model of the cavity with the crystal embedded. The z-cut face of the LN crystal (perpendicular to the yellow arrow) is aligned with the $z-$axis of the SRF cavity. **(b)** Schematic view of the experimental setup in the dilution refrigerator. **(c)** Electric field distributions of the TE01 and TM01 modes along the $z-$axis and the $xy-$plane.

Through a VNA (Vector Network Analyzer), the loaded quality factor of the cavity with the sample enclosed (Q_L) is measured. $1/Q_L$ is the sum of several components:

$$\frac{1}{Q_L} = \frac{1}{Q_0} + \frac{1}{Q_d} + \frac{1}{Q_{ext1}} + \frac{1}{Q_{ext2}} + \frac{1}{Q_{ext3}} + \frac{1}{Q_{ext4}}. \quad (1)$$

Q_0 is the intrinsic quality factor of the cavity, which takes into account the microwave loss on the cavity walls. $Q_{ext1,2,3,4}$ are the external quality factors of the couplers, which are calibrated at room temperature. In our experiments, the ports 3 and 4 are decoupled from the cavity such that $\frac{1}{Q_{ext3,4}} \to 0$. The other two couplers are tuned in such a way that the cavity is undercoupled. Q_d is the dielectric quality factor, i.e. the energy stored in the cavity (W) over the power dissipated in the dielectric sample (P_d), multiplied by the resonant frequency (ω):

$$Q_d = \frac{\omega W}{P_d} = \frac{1}{p \times \tan\delta}, \quad (2)$$

where, p is the filling factor of the dielectric material, i.e. the energy stored in the sample divided by the total stored energy in the whole cavity. The filling factor also depends on the dielectric permittivity of the crystal (ε_r), and it is different for each of the modes excited in the cavity.

Once the dilution refrigerator reaches the superconducting critical temperature of aluminum ($T_C = 1.2$ K), the microwave loss on the cavity's walls are negligible compared to the dielectric loss in the LN sample ($Q_0 >> Q_d$). The unloaded quality factor (Q_{UL}) is therefore calculated as:

$$\frac{1}{Q_{UL}} = \frac{1}{Q_L} - \frac{1}{Q_{ext1}} - \frac{1}{Q_{ext2}} \simeq \frac{1}{Q_d}. \quad (3)$$

The complex permittivity in isotropic materials can be written as $\varepsilon = \varepsilon_0\varepsilon_r = \varepsilon_0\varepsilon'_r(1 - j\tan\delta)$. The relative permittivity in anisotropic non-centrosymmetric crystals such as LN is instead a tensor:

$$\varepsilon_r = \begin{pmatrix} \varepsilon_\perp & 0 & 0 \\ 0 & \varepsilon_\perp & 0 \\ 0 & 0 & \varepsilon_\parallel \end{pmatrix}, \quad (4)$$

where, $\perp$ and $\parallel$ refer to the components perpendicular and parallel to the principal axis of the crystal, respectively [26]. The frequency shifts in resonant modes are proportional to the changes in the dielectric constant:

$$\Delta f = \frac{df}{d\varepsilon_\perp}\Delta\varepsilon_\perp + \frac{df}{d\varepsilon_\parallel}\Delta\varepsilon_\parallel, \quad (5)$$

where $\frac{df}{d\varepsilon_{\perp,\parallel}}$ are calibration constants derived from electromagnetic (EM) simulations for each of the microwave modes. With the dielectric crystal occupying most of the electromagnetic volume, losses are mainly concentrated in the crystal. Therefore, with $Q_L \sim 10^5$, the measurement's resolution in the evaluation of the dielectric constant is up to $\delta\varepsilon = 0.01$.

The z-cut face is perpendicular to the $z-$axis of the cavity which is the principal axis of the crystal (as in Fig. 2(a)). Among the various modes excited in the cavity, we monitor the TM01 and TE01 modes. The electric field distributions along the $z-$axis and the $xy-$plane are shown in Fig. 2(c). While the electric field of the TM01

mode is parallel to the $z-$axis, the electric field of the TE01 mode has components only in the $xy-$plane. For each mode, the dielectric loss tangent is evaluated as:

$$\frac{1}{Q_d} = p_\perp \tan\delta_\perp + p_\parallel \tan\delta_\parallel. \tag{6}$$

For TM and TE modes, the electric field is aligned to the $\parallel$ or $\perp$ planes, respectively [26]. Hence, we obtain:

$$\begin{aligned} \frac{1}{{Q_d}^{(TE)}} &= p_\perp \tan\delta_\perp, \\ \frac{1}{{Q_d}^{(TM)}} &= p_\parallel \tan\delta_\parallel. \end{aligned} \tag{7}$$

Measurements. Transmission parameters ($S21$) of TE and TM modes are measured using a VNA. The loaded quality factor is computed as $Q_L = \frac{f_{res}}{BW}$, where BW is the 3dB bandwidth. The 3dB bandwidth is estimated by applying a phase correction to rotate the in-phase and quadrature circle, canceling the detuning angle (δ_L). Then, the bandwidth is computed as the difference between f^+ and f^-: the locus point in which the absolute value of the imaginary part of S21 is at a maximum, corresponding to two vectors with arguments of $\phi_L = \pm\pi/4$ [27, 28], as shown in 3(a-b).

Measurements of external and loaded quality factors are shown in Fig. 3(c-d). As $Q_0 >> Q_d$[2]the quality factor of the dielectric sample is calculated as in Eq. (3). Frequency shifts are monitored, and changes in the electrical permittivity are referenced to the real part of the electrical permittivity at room temperature $\varepsilon_r = (42.5,\ 42.5,\ 26)$ [15, 16].

The filling factors ($p_\perp$ and $p_\parallel$) are computed through EM simulations using the values of the measured ε_r at 50 mK. To complete the analysis, the loss tangent is calculated from Eq. (7). The measurements of the relative permittivity and the loss tangent at T <500 mK, which are the main findings of this paper, are displayed in Fig. 3(e-f).

We confirm that the loss tangent of LN is in the order of 10^{-5} at microwave frequencies, and notably, we narrow the uncertainty range. In particular, we obtain $\tan\delta_\perp = 1.73\times10^{-5}$ and $\tan\delta_\parallel = 1.28\times10^{-5}$ at 50 mK. Main design parameters and measurements results are summarized in Table I.

Furthermore, we acquire few data points of a TE-like higher-order mode (HOM). The electrical field of this resonant mode propagates mainly on the xy-plane, but there are also components on the $z-$axis at a frequency of 9.5 GHz. The resulting loss tangent falls in between $\tan\delta_\perp$ and $\tan\delta_\parallel$ (Fig. 3(c) and Fig. 3(f)).

Error Analysis. The primary sources of error in the presented analysis are identified in the external quality factors and in the filling factors. To evaluate the uncertainty in the estimation of Q_{ext}, we compared measured and simulated values. We simulated Q_{ext} based on the knowledge of the antenna position and material properties. Then, we measured Q_{ext} through reflection on the 4-port cavity. These measurements show that additional radiations might be present, particularly for the TM01 mode, which propagates on the $z-$axis. Therefore, simulated and measured values are considered as the two extreme cases. We calculate Q_d from Eq. (3) for both cases, and we found the uncertainty of Q_d ($\delta(Q_d)$) for the TM and TE modes.

The uncertainty in the measurement of the loss tangent is derived as a combination of the estimation of the dielectric loss and the filling factor:

$$\frac{\delta(\tan\delta)}{\tan\delta} = \sqrt{\left(\frac{\delta(p)}{p}\right)^2 + \left(\frac{\delta(Q_d)}{Q_d}\right)^2}. \tag{8}$$

The uncertainty in the filling factor ($\delta(p)$) is also estimated through EM simulations. We consider an extreme case, in which the crystal is misaligned in the cavity with an offset of 0.5 mm. The total uncertainty is represented by the shaded area in Fig. 3(f). The results of the error analysis are listed in Table II.

TABLE I. Main design parameters and measurements results.

Parameter	Value	Unit
LN sample	$6\times6\times6$	mm
Cavity ($D\times H$)	11.2×34.5	mm
$f^{(TE01)}$	7.2	GHz
$f^{(TM01)}$	7.6	GHz
$df/d\varepsilon_\perp$	-40.603	MHz
$df/d\varepsilon_\parallel$	-64.637	MHz
$\varepsilon_\perp$	47	
$\varepsilon_\parallel$	28	
$p_\perp$ (50 mK)	92.3	%
$p_\parallel$ (50 mK)	46.3	%
$\tan\delta_\perp$ (50 mK)	1.73×10^{-5}	
$\tan\delta_\parallel$ (50 mK)	1.28×10^{-5}	

TABLE II. Estimated uncertainties.

Variable (V)	$\delta(V)/V$	$\delta(V)$
Q_d (TE01)	0.14	$\sim 8\times10^3$
Q_d (TM01)	0.15	$\sim 2.6\times10^4$
$p_\perp$	0.002	0.19
$\tan\delta_\perp$	0.14	$\sim 0.24\times10^{-5}$
$p_\parallel$	0.049	2.22
$\tan\delta_\parallel$	0.16	$\sim 0.21\times10^{-5}$

Loss Channels. The microwave loss in a piezoelectric dielectric sample may include the TLS (two-level-system) loss, the quasi-particle loss, the piezoelectric loss, and others [29]. To investigate the loss mechanisms in the LN sample, we analyze the dielectric quality factor of

[2] It is noted that the surface of the aluminum cavity was treated with buffered chemical polishing (BCP), removing 10 µm on the surface to reduce the losses on the superconducting cavity's walls.

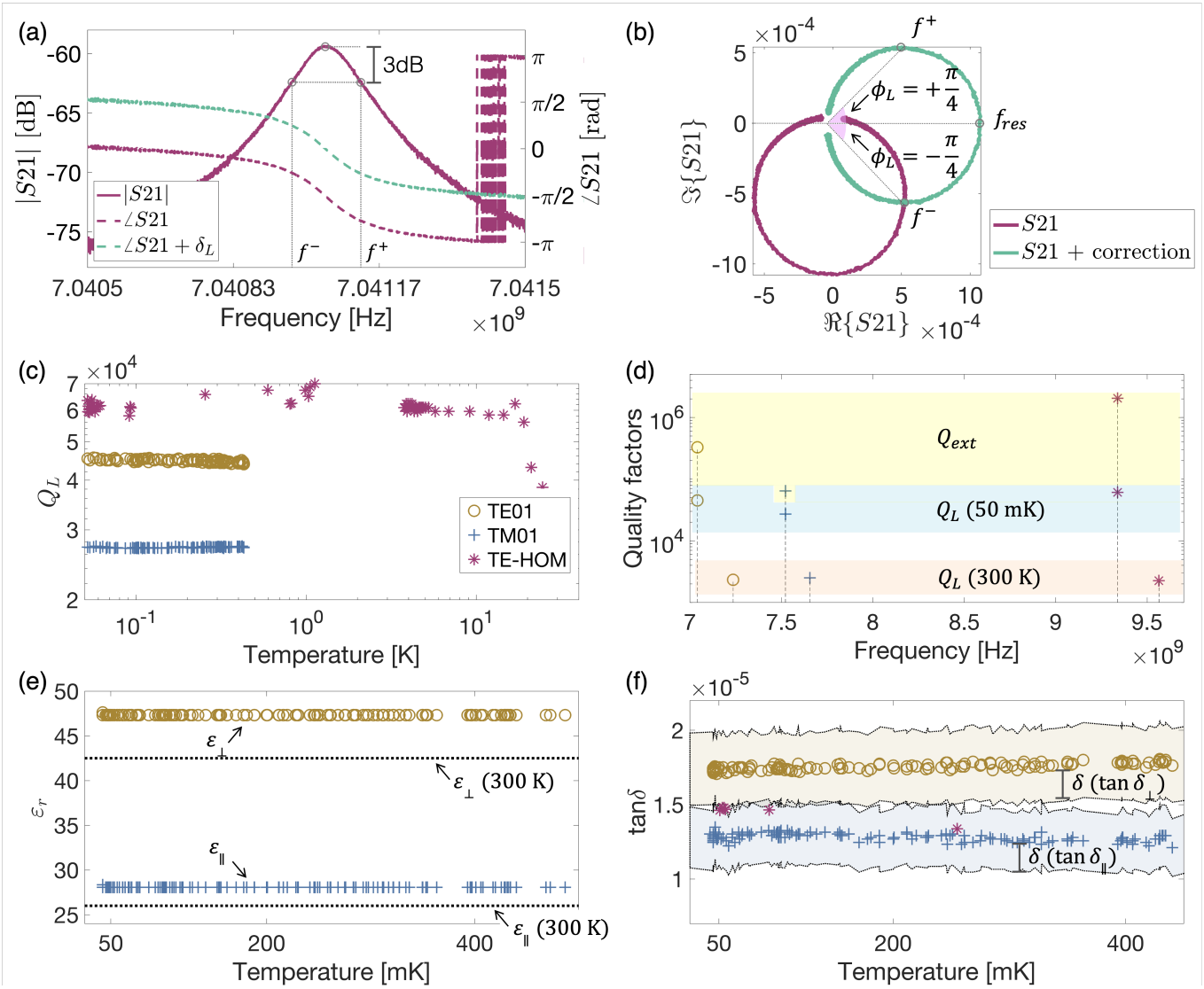


FIG. 3. **(a)** Magnitude and phase components of the S21 parameter. A phase correction is applied to cancel the detuning angle. **(b)** In-phase and quadrature components of the S21 parameter before and after the phase correction. Relevant RF parameters for the evaluation of the loaded quality factor are noted. **(c)** Loaded quality factor vs. temperature. **(d)** External quality and loaded quality factors at room temperature and at cryogenic temperatures, for each mode. **(e)** Measured permittivity vs. temperature. **(f)** Measured loss tangent vs. temperature. The total uncertainty is represented by the shaded area.

the TM mode versus the temperature (Fig. 4(a)). The weak temperature dependence of Q_d indicates that the quasi-particle loss is negligible in the overall cavity [29]. We then measure the quality factor at different input power levels. The average number of photons stored in the cavity $\langle n \rangle$ is determined through the transmitted power: $P_t Q_{ext2} = \hbar\omega^2 \langle n \rangle$, with $P_t = P_{in} - P_r - P_{loss}$, where P_{in} is the input power, P_r is the reflected power at Port 1, P_t is the power transmitted to Port 2, and P_{loss} is the power dissipated in the cavity [20, 30]. Fig. 4(b) displays Q_d versus the average number of photons stored in the cavity $\langle n \rangle$ at a fixed temperature of 80 mK. We observe that the dielectric quality factor increases with the number of photons. This is clear evidence of the presence of TLS as a source of dissipation, because the TLS is saturated at high RF power [18, 29]. Moreover, a temperature-independent piezoelectric loss and other types of unknown losses may exist. Further studies may be carried out to disentangle TLS and non-TLS mechanisms by precisely scanning the temperature and amplitude of the microwave field in the cryostat.

Conclusions and Outlook. Lithium niobate and other electro-optic dielectrics are being recognized as promising materials for quantum computing and sensing. We present findings on evaluating the complex electromagnetic permittivity of lithium niobate. Using a resonant-type method, we determined the loss tangent and the relative permittivity at millikelvin temperatures with un-

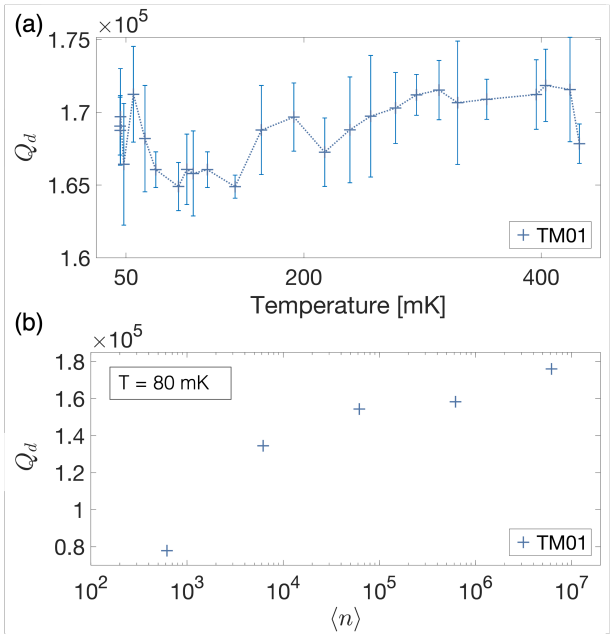


FIG. 4. **(a)** Losses in the LN crystal as a function of temperature. The error bars represent the standard deviation of the data acquired and analyzed. The input power is P_{in} =−52 dBm. **(b)** Losses in the LN crystal as a function of the average number of photons. P_{in} spans from −92 to −52 dBm.

precedented accuracy. We measured the parallel and perpendicular components of the loss tangent to be $(1.28 \pm 0.21) \times 10^{-5}$ and $(1.73 \pm 0.24) \times 10^{-5}$, respectively. These measurements are critical to devise applications that include coherent frequency conversions of microwave-optical photons. This project motivates further investigations to understand better the loss mechanisms of lithium niobate and other noncentrosymmetric crystals and explore the low-power limit. Future studies include measurements in the broader frequency regime, which shall be enabled by tunable cavities.

Acknowledgments. This manuscript has been authored by Fermi Research Alliance, LLC under Contract No. DE-AC02-07CH11359 with the U.S. Department of Energy, Office of Science, Office of High Energy Physics. This work is funded by the Fermilab's Laboratory Directed Research and Development (LDRD) program. This research used resources of the U.S. Department of Energy, Office of Science, National Quantum Information Science Research Centers, Superconducting Quantum Materials and Systems Center (SQMS) under contract number DE-AC02-07CH11359. The NQI Research Center SQMS contributed by supporting the design of SRF cavities and access to facilities. The authors would like to acknowledge help with the experimental setup from Roman Pilipenko and Geev Nahal Gelehpordsari, help with the mechanical design from Oleg V. Pronitchev, and help with cavity production from Edward D. Pieszchala and the Fermilab's village machine shop.

[1] R. Weis, and T. Gaylord, Lithium niobate: Summary of physical properties and crystal structure, Appl. Phys. A 37, 191-203 (1985)
[2] X. Han, W. Fu, C. Zou, L. Jiang, and H. Tang, Microwave-optical quantum frequency conversion, Optica 8, 1050-1064 (2021)
[3] N. Lauk, N. Sinclair, S. Barzanjeh, J. Covey, M. Saffman, M. Spiropulu, and C. Simon, Perspectives on quantum transduction, Quantum Sci. Technol. 5, 020501 (2020)
[4] C. Wang, I. Gonin, A. Grassellino, S. Kazakov, A. Romanenko, V. Yakovlev, and S. Zorzetti, High-efficiency microwave-optical quantum transduction based on a cavity electro-optic superconducting system with long coherence time, npj Quantum Inf. 8, 149 (2022)
[5] M. Hossein-Zadeh, and A. Levi, 14.6-GHz $LiNbO_3$ microdisk photonic self-homodyne RF receiver, IEEE Trans. Microw. Theory Tech. 54, 821-831 (2006)
[6] S. Danti, B. Azimi, M. Candito, A. Fusco, M. Sorayani Bafqi, C. Ricci, M. Milazzo, C. Cristallini, M. Latifi, G. Donnarumma, and Others Lithium niobate nanoparticles as biofunctional interface material for inner ear devices, Biointerphases 15, 031004 (2020)
[7] N. Lauk, N. Sinclair, S. Barzanjeh, J. Covey, M. Saffman, M. Spiropulu, and C. Simon, Perspectives on quantum transduction, Quantum Sci. Technol. 5, 020501 (2020)
[8] M. Zhang, B. Buscaino, C. Wang, A. Shams-Ansari, C. Reimer, R. Zhu, J. Kahn, and M. Lončar, Broadband electro-optic frequency comb generation in a lithium niobate microring resonator, Nature 568, 373-377 (2019)
[9] M. Tsang, Cavity quantum electro-optics, Phys. Rev. A 81, 063837 (2010)
[10] W. Hease, A. Rueda, R. Sahu, M. Wulf, G. Arnold, H. Schwefel, and J. Fink, Bidirectional electro-optic wavelength conversion in the quantum ground state, PRX Quantum 1, 020315 (2020)
[11] R. Sahu, L. Qiu, W. Hease, G. Arnold, Y. Minoguchi, P. Rabl, and J. Fink, Entangling microwaves with optical light, arXiv:2301.03315 (2023)
[12] M. Mirhosseini, A. Sipahigil, M. Kalaee, and O. Painter, Superconducting qubit to optical photon transduction, Nature 588, 599-603 (2020)
[13] M. Jazbinšek, and M. Zgonik, Material tensor parameters of LiNbO3 relevant for electro-and elasto-optics, Appl. Phys. B 74, 407-414 (2002)
[14] C. Cena, A. Behera, and B. Behera, Structural, dielectric, and electrical properties of lithium niobate microfibers, J. Adv. Ceram. 5, 84-92 (2016)
[15] Y. Ohmachi, K. Sawamoto, and H. Toyoda, Dielectric properties of LiNbO3 single crystal up to 9 Gc, Jpn. J. Appl. Phys. 6, 1467 (1967)
[16] S. Abrahams, Properties of lithium niobate, New York 236 (1989)
[17] M. Goryachev, N. Kostylev, and M. Tobar, Single-photon level study of microwave properties of lithium niobate at millikelvin temperatures, Phys. Rev. B 92, 060406 (2015)
[18] E. Wollack, A. Cleland, P. Arrangoiz-Arriola, T.

McKenna, R. Gruenke, R. Patel, W. Jiang, C. Sarabalis, and A. Safavi-Naeini, Loss channels affecting lithium niobate phononic crystal resonators at cryogenic temperature, Appl. Phys. Lett. 118, 123501 (2021)

[19] A. Romanenko, R. Pilipenko, S. Zorzetti, D. Frolov, M. Awida, S. Belomestnykh, S. Posen, and A. Grassellino, Three-dimensional superconducting resonators at T < 20 mK with photon lifetimes up to $\tau = 2$ s, Phys. Rev. Appl. 13, 034032 (2020)

[20] A. Romanenko, and D. Schuster, Understanding quality factor degradation in superconducting niobium cavities at low microwave field amplitudes, Phys. Rev. Lett. 119, 264801 (2017)

[21] M. Checchin, D. Frolov, A. Lunin, A. Grassellino, and A. Romanenko, Measurement of the low-temperature loss tangent of high-resistivity silicon using a high-Q superconducting resonator, Phys. Rev. Appl. 18, 034013 (2022,9)

[22] S. Zorzetti, C. Wang, I. Gonin, S. Kazakov, I. Nekrashevich, and V. Yakovlev, Methods for microwave characterization of electro-optic crystals for quantum transduction, 2022 IEEE International Conference On Quantum Computing And Engineering (QCE), 410-414 (2022)

[23] C. McRae, H. Wang, J. Gao, M. Vissers, T. Brecht, A. Dunsworth, D. Pappas, and J. Mutus, Materials loss measurements using superconducting microwave resonators, Rev. Sci. Instrum. 91, 091101 (2020)

[24] J. Krupka, K. Derzakowski, M. Tobar, J. Hartnett, and R. Geyer, Complex permittivity of some ultralow loss dielectric crystals at cryogenic temperatures, Meas. Sci. Technol. 10, 387 (1999)

[25] D. Creedon, Y. Reshitnyk, W. Farr, J. Martinis, T. Duty, and M. Tobar, High Q-factor sapphire whispering gallery mode microwave resonator at single photon energies and millikelvin temperatures, Appl. Phys. Lett. 98, 222903 (2011)

[26] C. Li, C. Wu, and L. Shen, Complex Permittivity Measurement of Low-Loss Anisotropic Dielectric Materials at Hundreds of Megahertz, Electronics 11, 1769 (2022)

[27] D. Kajfez, and J. H. Eugene, Q-factor measurement with network analyzer, IEEE Trans. Microw. Theory Tech. 32.7, 666-670 (1984)

[28] F. Caspers, and P. Kowina, RF measurement concepts, CERN (2014)

[29] M. Scigliuzzo, L. Bruhat, A. Bengtsson, J. Burnett, A. Roudsari, and P. Delsing, Phononic loss in superconducting resonators on piezoelectric substrates, New J. Phys 22, 053027 (2020)

[30] O. Melnychuk, A. Grassellino, and A. Romanenko, Error analysis for intrinsic quality factor measurement in superconducting radio frequency resonators, Rev. Sci. Instrum. 85, 124705 (2014)